Thin Solid Films 520 (2012) 5985–5990

Contents lists available at SciVerse ScienceDirect

Thin Solid Films

journal homepage: www.elsevier.com/locate/tsf

Crossover from dirty to clean superconducting limit in dc magnetron-sputtered thin Nb films

Oleksandr V. Dobrovolskiy *, Michael Huth

Physikalisches Institut, Goethe-Universität, Max-von-Laue-Str. 1, 60438 Frankfurt am Main, Germany

ARTICLE INFO

Article history:
Received 25 January 2012
Received in revised form 16 April 2012
Accepted 19 April 2012
Available online 11 May 2012

Keywords:
Epitaxial Nb films
DC magnetron sputtering
Clean and dirty superconducting limits
Critical temperature
Residual resistivity

ABSTRACT

High-quality Nb (110) thin films with residual resistance ratios up to 60 and critical temperatures $T_c \approx 9.27$ K have been prepared by conventional dc-magnetron sputtering on α-Al_2O_3 by careful selection of the sputtering conditions. This allowed for a systematic study of the influence of the growth rate on the structural quality and the superconducting properties of the films. The optimized growth conditions were revealed at the substrate temperature $T_s = 850$ °C, Ar pressure $P_s = 0.4$ Pa, and the growth rate $g \approx 0.5$ nm/s. The results of the films' structural characterization by X-ray diffraction, reflection high-energy electron diffraction, and atomic force microscopy are presented. In terms of the electron mean free path l and the superconducting coherence length ξ, deduced from the magneto-resistivity data, the clean superconducting limit ($l > \xi$) is realized in the high-purity films. For comparison, in impure Nb films sputtered at room temperature while keeping the rest of the sputtering parameters unvaried, the opposite dirty limit ($\xi \gtrsim l$) ensues. The merits of these findings are discussed in the context of the demands of present-day fluxonics devices regarding the normal-state and flux-flow properties of superconducting films they are made of.

1. Introduction

The superconducting properties of thin films are known to differ substantially from those of bulk materials they are made of. This is caused by a larger amount of defects in the crystalline structure in comparison with the bulk, that reduces the electron mean-free path l and causes peculiarities in the electron–electron [1] and electron–phonon [2] interactions. If a specimen is made of a superconductor, like in the case of Nb, its normal-state and mixed-state properties become very sensitive to the structural quality [3], purity [4], and the film thickness d [5,6].

The correlation between the structural and superconducting properties in thin films of Nb represents a widely studied problem [3–15]. In particular, the influence of the lattice parameter a, grain size D, and surface roughness Δd on the critical temperature T_c and the normal-state resistivity ρ_n has been a matter of thorough experimental investigations on nano-granular disordered [7–9], high-purity [10], and dirty [11] Nb films. Different growth techniques have been used in these works [3–15]. For the growth of high-purity thin Nb films revealing outstanding structural quality, the molecular beam epitaxy (MBE) method has been shown to be the most efficient as compared to others [12–14], see also [15] for a topical review. At the same time, much less attention has been paid to optimize the growth conditions with emphasis on the tunability of the normal-state and superconducting properties of the films prepared by means of sputter deposition, in particular, by dc magnetron sputtering.

Our motivation to optimize the growth parameters of Nb sputtered films is as follows. On the one hand, due to their robust superconductivity, thin Nb films are very suitable for fundamental investigations of vortex matter, such as the study of flux-flow properties [3], scattering mechanisms [16], and the vortex dynamics in as-grown and nanostructured specimens [17–19]. On the other hand, Nb is an ideal material for a number of applications such as hot-electron bolometer mixers [20], superconducting nanowire single-photon detectors [21], rapid single flux quantum logic [22], and other fluxonics devices [23]. It should be stressed that these devices put conflicting demands on the film properties. For instance, the superconducting nanowire single-photon detector is better, if made from 'dirty' superconducting films [21], whereas devices operating at high dissipation levels should be fabricated from 'clean' films, chiefly to reduce flux-flow losses.

In accordance with the Bardeen–Stephen model [24], the normal-state resistivity ρ_n and the dissipation by vortices in the mixed state, determined by the flux-flow resistivity ρ_f, are interrelated values, since $\rho_f \cong \rho_n(B/B_{c2})$. Here B is the external magnetic field and B_{c2} is the upper critical field. In the normal state, ρ_n is influenced by the film quality through the change of the electron mean free path l. In the mixed state, the purity of the film affects the superconducting coherence length, ξ. This becomes apparent through the upper critical field value, which at zero temperature equals $B_{c2}(0) = \Phi_0/2\pi\xi^2(0)$ [25], where Φ_0 is the magnetic flux quantum. By this way, in terms of ξ and l, one can consider two different regimes in a sample, depending on its quality: the superconducting clean limit when $l > \xi$ and the dirty limit when $l \lesssim \xi$.

* Corresponding author. Tel.: +49 69 798 47263.
E-mail address: Dobrovolskiy@Physik.uni-frankfurt.de (O.V. Dobrovolskiy).

0040-6090/$ – see front matter © 2012 Elsevier B.V. All rights reserved.
doi:10.1016/j.tsf.2012.04.083

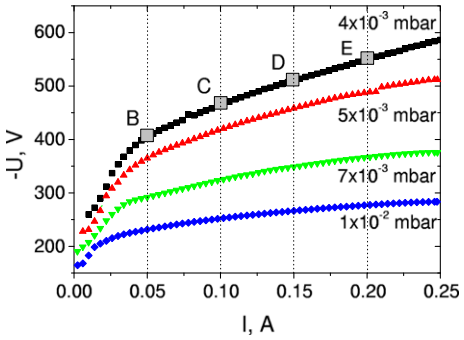

Fig. 1. Current–voltage characteristics in the cathode circuit of the dc magnetron sputtering setup at 850 °C for a series of pressures P_s, as indicated. Shown are operating points B, C, D, and E at the Ar pressure $P_s = 0.4$ Pa at a set of currents I providing a growth rate g of 0.5, 1, 1.5 and 2 nm/s, respectively. Sample B2, deposited at operating point B, which corresponds to a lowest growth rate still in the almost linear segment of the CVC, revealed the lowest residual resistivity and the highest T_c among all investigated (51 ± 1 nm-thick) films.

In the present work, we report details of preparation, characterization and results of magneto-transport measurements on Nb films fabricated by dc magnetron sputtering under non-optimal and optimized growth conditions with regard to the films' structural quality, as confirmed by X-ray diffraction, atomic force microscopy (AFM) inspection, and reflection high energy electron diffraction (RHEED) measurements. Depending on the structural quality, we call the films 'pure' and 'impure'. From the results of the transport measurements, in terms of l and ξ, our pure Nb films are clearly in the superconducting clean limit, whereas the opposite dirty limit is revealed in the impure samples.

2. Methods and techniques

For the film deposition a home-made dc magnetron sputtering setup, equipped with a 2" niobium target of 99.996% purity was used. The substrates are commercially available (CrysTec GmbH) one-side epi-polished pieces of α-Al_2O_3 ($11\bar{2}0$). Before use, the substrates, with a nominal size of $10 \times 10 \times 0.53$ mm^3 were passed through a series of ultrasound baths with cleaning solutions consisting of acetone, de-ionized water, and isopropanol. One substrate (referred to as sample A below) was also used to take the X-ray reflectivity data and to inspect its surface morphology. The substrates were mounted onto the holder by using a two-component epoxy resin (Eccobond 56). The substrate holder with mounted substrate was first degassed in Ar atmosphere at a pressure of 1×10^{-5} Pa at 900 °C for 30 min with the sputter system operating at a base pressure of less than 1×10^{-5} Pa. During the sputtering process the substrates were kept at 850 °C or at room temperature for one film (labeled below as F). All the films were sputtered in 99.999% Ar atmosphere at a pressure of 0.4 Pa. The films' thickness was inferred from the sputtering time after accurate calibration of the deposition rate on a number of Nb films. The current–voltage characteristics (CVC) in the cathode circuit of the sputtering setup are shown in Fig. 1. In the CVC, one can clearly distinguish a nonlinear region for $I \lesssim 0.05$ A and an almost linear segment at $I \gtrsim 0.05$ A. Since reproducible results are very hard to obtain in the nonlinear regime we focused on the current range above 0.05 A. In this range we present 4 representative samples grown at rates $g = 0.5; 1; 1.5; 2$ nm/s which are labeled B, C, D, and E, respectively. The same labels are used throughout the text to identify the samples whose properties are summarized in Table 1.

The microstructure of the sputtered films was investigated by means of both, low- and high-angle X-ray diffraction analysis. Diffraction data were collected from a high-resolution Bruker D8 MRD diffractometer, in a CuK_α parallel-beam configuration. Characteristic measurements with this instrument were performed at room temperature in air in symmetric reflection geometry. The software used to analyze the data was Bruker's Diffrac^{plus} Leptos software (v. 3.03).

For high-resolution morphology characterization, AFM under ambient conditions in non-contact mode was used. The films' thickness was confirmed by both, low-angle X-ray diffraction and AFM inspection. To examine the epitaxy in the films, post-growth RHEED measurements have been performed, in high-vacuum at 700 °C in a different vacuum chamber.

All the films from the second set were pre-patterned by standard photolithography followed by Ar ion-beam etching in order to define 4-contact bridges with a cross-area of 30×100 μm^2. Magneto-transport measurements were performed in a helium flow cryostat equipped with a 9 T superconducting solenoid and a variable temperature insert. The measurements were done by the four-probe method at fixed current.

3. Sample preparation

3.1. Sputtering conditions

Pinning is known to be strong in Nb films [3]. For the efficient manipulation of fluxons via artificially created anisotropic nanopatterns [19], detrimental background isotropic pinning in as-grown Nb films has to be avoided. As is well-known [26], the quality of thin films is determined chiefly by three parameters, namely the substrate temperature T_s, the growth rate g, and the pressure of the sputtering gas P_s, i.e., Ar in the present case. In accordance with [26], microstructure, structural coherence, and surface morphology of a film represent strongly interrelated properties which can be tuned to a large degree by varying the above-mentioned parameters. As a consequence, Nb films of high crystal quality can be prepared only under optimized growth conditions. In accordance with the growth mode considered by Thornton [26] and later on extended by Flynn [27], the optimal substrate temperature during the epitaxial growth should satisfy the condition $1/3T_m \lesssim T_s \lesssim 3/8T_m$, where T_m is the melting temperature in K of the material to be deposited. In the case of Nb, T_s is $800 \div 920$ °C. A further increase of T_s is thought to be counterproductive, since then oxygen may easier dissociate from the Al_2O_3 substrate in the interface region and cause oxidation of the Nb layer [15]. The increase of the Ar pressure during the sputtering process is known to cause an enhanced Ar inclusion into the film [4]. Besides, the film

Table 1
Structural parameters and superconducting properties of the samples. NA means 'not available'.

Sample	d, nm	Δd, nm	$\theta_{(110)}$, °	β, °	T_c, K	ΔT_c, K	RRR	ρ_n, μΩ cm	$H_{c2}(0)$, mT	$\xi(0)$, nm	l, nm
A	NA	0.3	37.78	0.08	NA	NA	NA	NA	NA	NA	NA
B1	47	0.7	NA	NA	9.07	<0.02	14	0.93	780	21	40
B2	52	0.7	38.52	0.22	9.14	<0.01	38	0.45	700	22	83
B3	60	0.7	NA	NA	9.23	<0.01	60	0.25	610	23	149
C	50	2	38.51	0.24	NA	NA	NA	NA	NA	NA	NA
D	52	3.5	38.55	0.25	NA	NA	NA	NA	NA	NA	NA
E	51	4.5	38.59	0.28	NA	NA	NA	NA	NA	NA	NA
F	54	2	38.48	0.30	8.32	0.15	2.7	9.9	1600	14	4

surface is known to be smoother when deposited at lower pressures, whereas at high pressures, columnar growth with intercolumnar gaps has been found [4]. At the same time, by increasing the incident atom energy and incident flux at fixed Ar pressure, the resulting effective increase of the substrate temperature right at the surface leads to higher adatom mobility [26]. Thereby, we kept $P_s = 0.4$ Pa, as the lowest pressure at which the plasma was stable and changed only the growth rate g in order to determine its influence on the films' structural quality.

3.2. Samples

3.2.1. First set of films

By using the growth rates of 0.5 ; 1 ; 1.5 ; 2 nm/s, four niobium films (B2, C, D, and E) with a thickness of 51 ± 1 nm have been sputtered as detailed in the caption of Fig. 1.

3.2.2. Second set of films

Two Nb films B1 and B3 with a thickness of 47 nm and 60 nm, respectively, have been sputtered. For these two films, the substrate temperature was 850 °C and the growth rate was 0.5 nm/s (operating point B). One additional film F has been sputtered with the same growth rate at room temperature (22 °C) for reference purposes. Other details of the preparation are the same as those from the first set.

4. Characterization of the samples

4.1. X-ray diffraction

X-ray diffraction data are shown in Fig. 2. Nb was found to grow (110)-oriented, as expected from the known epitaxial orientation relationship of Nb on sapphire [15]. The closed-packed (110) bcc plane therefore grows parallel to the $(11\bar{2}0)$ a-plane sapphire surface. For strain-free Nb layers the (110) peak position at the wavelength $\lambda = 1.5406$ Å is expected to be at 38.546°. In our films A–E, the magnitude of the (110) Bragg peak decreases while broadening with increase of growth rate from 0.5 nm/s to 2 nm/s. This is accompanied by a slight shift of the peak position toward larger θ. The broadening of the peak is attributed to two factors, namely the tendency to nanocrystallinity and the development of a texture in the plane of the substrate.

Film F, sputtered at room temperature, shows a very smooth (110) peak, which is shifted toward smaller angles. It should be noted that no peaks related to the presence of Nb oxide have been detected neither for the films sputtered at 850 °C nor for the film sputtered at room temperature. Nevertheless, the formation of an amorphous oxides Nb_2O_5, is known to occur at the top 2 nm of a 50 nm-thick Nb film [15]. This oxidized layer is formed during the first seconds after a film has been taken out from the sputtering setup. It serves as a protection layer preventing further oxidation of the film.

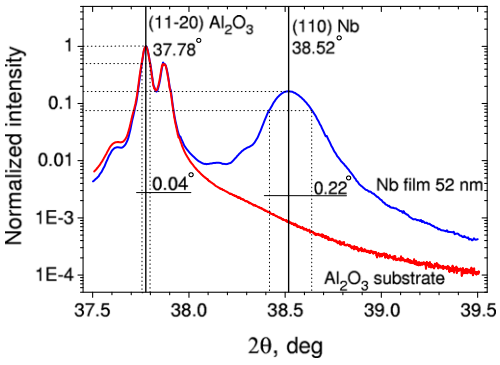

Fig. 3. First order specular X-ray scan of the 52 nm-thick Nb film B2 and the sapphire $(11\bar{2}0)$ substrate in logarithmic scale. Shown is the full width at half maximum by dashed lines, which is equal to 0.22°. For the high-angle side of the Nb(110) peak one can recognize Laue oscillations, indicative for the high structural order of the film.

In Fig. 3 we plot the data for the 52 nm-thick Nb film B2 demonstrating the most intense and narrow (110) peak among all films from the first set. The reflection from the sapphire substrate is shown for reference purposes. We deduce a full width at half maximum (FWHM) of $\beta = 0.22°$, which is fully in-line with typical values measured on the highest quality epitaxial films grown by MBE [15]. For comparison, the width of the narrow (110) sapphire peak and its satellite due to CuK_β is 0.08°. One also can recognize Laue oscillations at the high-angle side of the Nb (110) peak. These oscillations arise from a well-defined number of coherently scattering planes, and their occurrence is indicative for the high structural quality of the film.

Fig. 4 shows the reflection intensity in logarithmic scale for scattering angles larger than the critical angle of the total external reflection [θ_c(Nb) = 0.39°]. Several interference maxima can be identified so that an accurate film thickness determination is possible. The data were simulated by using two fitting parameters: the film thickness and the surface roughness, as $d = 52$ nm and $\Delta d = 0.7$ nm, respectively. While the thickness determines chiefly the number and the position of oscillations, the roughness causes the damping of the oscillations with increasing angle. The formation of an oxide layer has not been taken into account in the simulation as no over-modulation due to the very thin oxide layer has been detected (as peculiar to thinner films [12,29]). We did not succeed to reproduce the sharp minima in the reflectivity data. This difficulty has also been reported by other authors [12] and is commonly attributed to the presence of inhomogeneous strain.

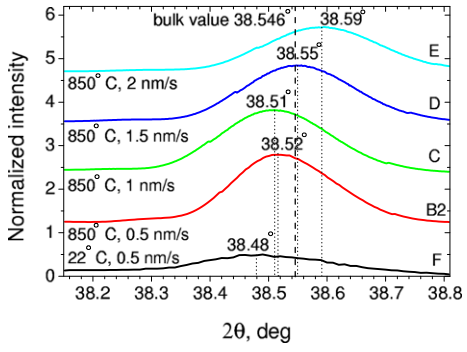

Fig. 2. Longitudinal scans of the (110) Bragg peak of Nb films sputtered under different conditions, as indicated next to the curves ($\lambda = 1.54$ Å). Film thickness in all cases is 51 ± 1 nm. Along the vertical axis, an offset of 1.2 is used to facilitate comparison. The vertical dotted lines show the (110) Bragg peak positions.

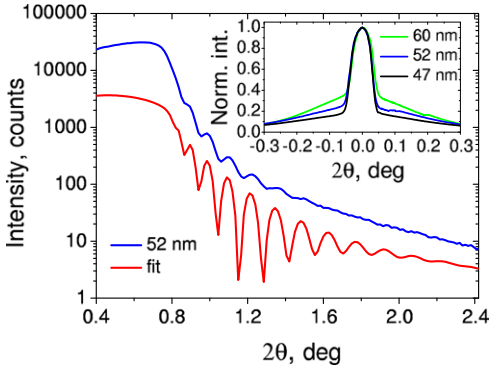

Fig. 4. Small angle X-ray reflectivity data for sample B2 with 52 nm thickness. The fit is shifted downwards by a factor of ten for ease of comparison. Inset: Transverse scans of the Nb (110) Bragg reflection for different Nb thicknesses demonstrating the presence of a sharp and broad component, as expected for epitaxial films [13,28].

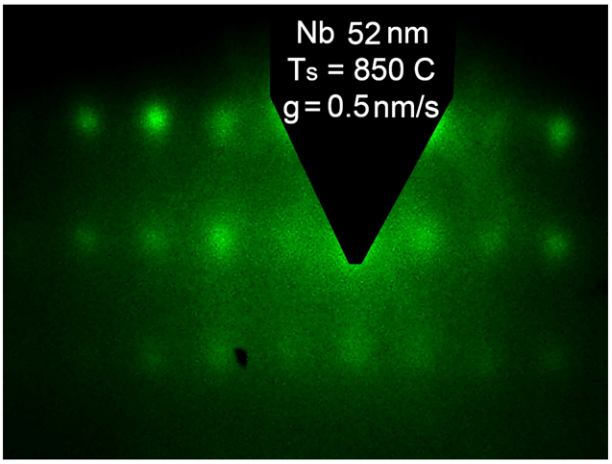

Fig. 5. RHEED pattern taken after the deposition of a 52-nm thick Nb film (B2) grown at operating point B (clean superconducting limit).

Typical transverse (rocking curve) scans for the films B1, B2, and B3 are shown in the inset to Fig. 4. Films of different thicknesses show a sharp specular and a broad diffusive component in transverse scans at the Bragg position (110). The FWHM of the sharp component is $\Delta\omega_{sharp} = 0.07^{\circ}$. The FWHM of the broad component $\Delta\omega_{sharp}$ is 0.35°. This background component is a characteristic of rotational disorder [28] and accounts for the orientational distribution of epitaxial crystallites (mosaicity). The width of the rocking curve gives as a lower limit for the lateral domain size $L = 2\pi/d\sin\omega$, i.e., $L_{narrow} = 103$ nm, whereas $L_{broad} = 21$ nm.

4.2. RHEED and AFM analysis

RHEED measurements were performed on film B2 with a thickness of 52 nm which, as will be shown in the next subsection, is in the clean superconducting limit. The RHEED pattern is shown in Fig. 5 and confirms the epitaxial growth of the film.

The sequence of AFM images in Fig. 6 reveals a pronounced morphology change as Nb is grown on Al_2O_3 at various growth rates. The surface roughness increases with increasing growth rate. The roughness of sample B2 is $\Delta d < 0.8$ nm, which is in reasonable agreement with $\Delta d = 0.7$ nm used in the simulation of the small angle X-ray reflectivity data. Further details of the films morphology are given in the caption of Fig. 6.

Taking the above-mentioned considerations into account, we find that the experimental reflectivity data confirm the highly ordered

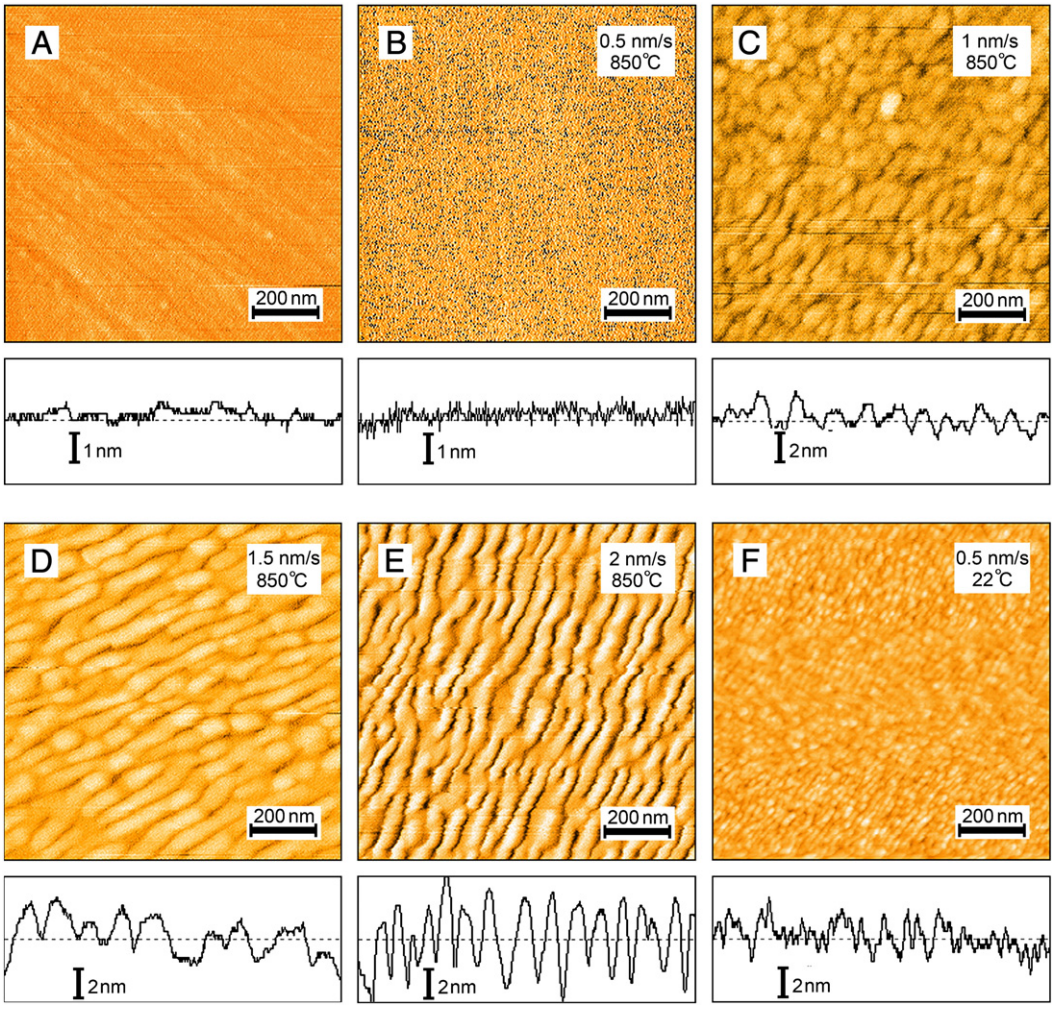

Fig. 6. AFM images of the surfaces of the Al_2O_3 substrate (A) and Nb films sputtered at $T_s = 850$ °C at different growth rates (B–E), as indicated. All the films have a thickness of 51 ± 1 nm. The area of each micrograph is $1 \times 1\ \mu m^2$. Typical line scans are shown below the AFM images. The surface morphology shows the development of long narrow grains with increase of the deposition rate. The film roughness is found to increase systematically with the increase of the growth rate. The flattest morphology is observed for the film sputtered at condition B; this is accompanied by a close-to-bulk T_c and a very small ρ_n, as representative for the clean superconducting limit. The sample grown at room temperature (F) shows a granular morphology, with spherical granules of a typical diameter of 20 nm without any indication of a preferential in-plane orientation. Sample F exhibits the dirty superconducting limit.

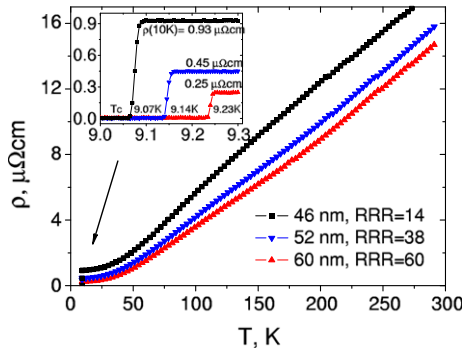

Fig. 7. Zero-field cooling curves $\rho(T)$ for Nb films B1, B2, and B3 in the clean superconducting limit. The residual resistivity ratio is determined as RRR $= \rho_{300\,K}/\rho_{10\,K}$.

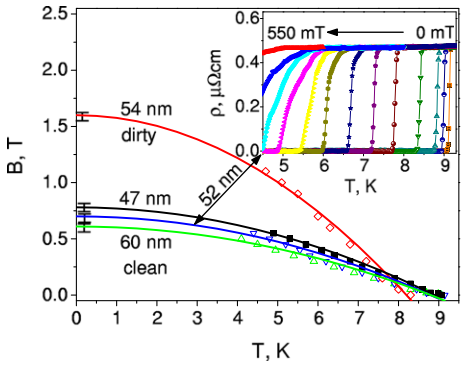

Fig. 9. The temperature dependence $\mu_0 H_{c2}(T)$ for the three clean and one dirty Nb films. The $\mu_0 H_{c2}(0)$ values are estimated by fitting the standard expression $H_{c2}(T) = H_{c2}(0)[1-(T/T_c)^2]$. Error bars are also shown.

growth of (110) Nb onto $(11\bar{2}0)$ sapphire, for the films sputtered under condition B. At the same time, the film grown at room temperature shows a high granularity. How these structural characteristics correlate with the superconducting properties is discussed in the next subsection.

5. Superconducting properties and discussion

Typical zero-field cooling curves for the high-quality ('clean') Nb films are shown in Fig. 7. The $\rho(T)$ curves have been measured with the four-point dc resistive method. The critical temperatures were determined as the midpoint of the resistive transition $\rho(T)$. As is evident from the figure, the clean Nb films (B1, B2, and B3) demonstrate outstanding superconducting properties, namely a critical temperature T_c very close to the bulk value of 9.27 K for Nb, and a very small residual resistivity value of $\rho_{10\ K} < 0.5\,\mu\Omega$ cm. The sharp transition widths (<0.01 K) are additional strong indicators of homogeneous and high-quality films. The residual resistivity ratio (RRR $= 14 \div 60$) is defined here as the ratio of the resistivity at 300 K to that at 10 K and again reflects the overall crystal quality of the films. The measured RRR values on the pure Nb films belong to the largest reported so far for thin Nb films. For completeness, bulk Nb crystals with RRR in the range of $50 \div 1000$ are commercially available.

The values of ρ_n at 10 K are within 1% accuracy equal to those close to T_c in the normal state. Consequently, we used the $\rho_n(10\,K)$ values to estimate the electron mean free path l from the material constant $\rho_0 l = 3.72 \times 10^{-6}\,\mu\Omega\,cm^2$ for Nb which is widely used [5,7]. The estimated l values for several films are listed in Table 1. It can be seen from this table that the T_c values for the films sputtered under condition B (B1, B2, and B3) are about equal to that of bulk single crystals. This allows us to call them 'optimized' with respect to the superconducting properties of these films. It can be seen that the RRRs vary systematically with the thickness: The thinnest films always have the smallest RRRs.

A typical zero-field cooling curve for the low-quality ('dirty') Nb film (F) is shown in Fig. 8. Important consequences of the pronounced granularity are a high resistivity value of $\rho_n = 9.9\,\mu\Omega$ cm, a reduced critical temperature of $T_c = 8.32$ K with $\Delta T_c = 0.15$ K and a low RRR value of about 2.7. A significant contribution to the resistivity is attributed to the grain boundaries.

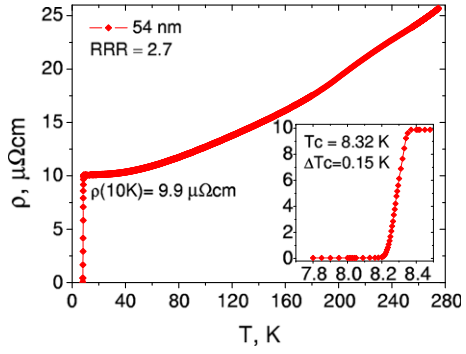

Fig. 8. Zero-field cooling curve $\rho(T)$ for the Nb film (F) in the dirty superconducting limit.

We have also measured a series of $\rho(T)$ curves in different perpendicular magnetic fields $B = 0 \div 1.2$ T for the three clean and the dirty Nb films. The results are shown in Fig. 9. The upper critical field was determined as the respective onset of the $\rho(H)$ curves. From the $H_{c2}(0)$ values as determined by fitting the standard expression $H_{c2} = H_{c2}(0)[1-(T/T_c)^2]$ we extracted the coherence length value $\xi(0)$ [25]. The values of $\xi(0)$ were found to be around 22 nm for the clean limit samples and 14 nm for the sample in the dirty limit. The inaccuracy in the estimation of $\xi(0)$ is ± 1 nm for all the films.

6. Conclusion

By careful selection of the sputtering conditions we have been able to reproducibly prepare Nb thin films of the highest quality. This allowed us to systematically study the influence of the growth rate on the structural quality and the superconducting properties of the films. Two main conclusions emerged from this study: First, dc magnetron sputtering is well-suited to prepare Nb films in a wide range of structural quality. The degree of structural disorder can be clearly correlated with the superconducting properties.

Second, under optimized growth conditions, dc-sputtered Nb films with a thickness of about 50 nm demonstrate outstanding superconducting properties, which are fully comparable with films grown by molecular beam epitaxy. In particular, their superconducting transition is very sharp ($\Delta T < 0.01$ K), the residual resistivity value is very low $\rho_{10\,K} < 0.5\,\mu\Omega$ cm, and T_c is very close to the bulk value. Typical RRR values up to 60 have been obtained.

It should be noted that clean-limit Nb films substantiate an ideal sample basis to investigate, e.g., physics in the area of directed vortex motion, once such films have been nanostructured with a system of grooves or lines in the spirit of Ref. [19]. In this case the critical current anisotropy must be described in the limit of pure anisotropic pinning. Another interesting topic is a comparative study of the Hall effect in 'clean' and 'dirty' Nb films. Research along these lines is currently under way.

Acknowledgments

The authors are very grateful to Jörg Franke for the design and the assembly of the dc magnetron sputtering setup. Oleksandr Foyevtsov is sincerely thanked for discussions of the X-ray data. Roland Sachser is acknowledged for the software written. Albrecht Köhler is thanked for his help with the RHEED measurements. Useful discussion with Valerij A. Shklovskij is acknowledged. O.V.D. is grateful to the Deutsche

Forschungsgemeinschaft (DFG) for financial support through grant no. DO 1511/2-1.

References

[1] B. Altshuler, A. Aronov, D. Khmelnitsky, J. Phys. C 15 (1982) 7367.
[2] A. Schmid, Z. Phys. A 259 (1973) 421.
[3] C. Peroz, C. Villard, Phys. Rev. B 72 (2005) 014515.
[4] C. Wu, Thin Solid Films 64 (1979) 103.
[5] A. Gubin, K. Il'in, S. Vitusevich, M. Siegel, N. Klein, Phys. Rev. B 72 (2005) 064503.
[6] K. Il'in, D. Rall, M. Siegel, A. Engel, A. Schilling, A. Semenov, H.-W. Huebers, Physica C 470 (2010) 953.
[7] D. Hazra, M. Mondal, A. Gupta, Physica C 469 (2009) 268.
[8] S. Bose, P. Raychaudhuri, R. Banerjee, P. Vasa, P. Ayyub, Phys. Rev. Lett. 95 (2005) 147003.
[9] S. Bose, P. Raychaudhuri, R. Banerjee, P. Ayyub, Phys. Rev. B 74 (2006) 224502.
[10] R. Banerjee, E. Sperling, G. Thompson, H. Fraser, S. Bose, P. Ayyub, Appl. Phys. Lett. 82 (2003) 4250.
[11] V. Lacquaniti, S. Maggi, E. Monticone, R. Steni, Phys. Status Solidi A 151 (1995) 335.
[12] C. Sürgers, C. Strunk, H.V. Löhneysen, Thin Solid Films 239 (1994) 51.
[13] B. Wölfing, K. Theis-Bröhl, C. Sutter, H. Zabel, J. Phys. Condens. Matter 11 (1999) 2669.
[14] M. Allain, B. Heuser, Phys. Rev. B 72 (2005) 054102.
[15] A. Wildes, J. Mayer, K. Theis-Bröhl, Thin Solid Films 401 (2001) 7.
[16] A. Leo, G. Grimaldi, R. Citro, A. Nigro, S. Pace, R. Huebener, Phys. Rev. B 84 (2011) 014536.
[17] M. Huth, K. Ritley, J. Oster, H. Dosch, H. Adrian, Adv. Funct. Mater. 12 (2002) 333.
[18] O. Soroka, V. Shklovskij, M. Huth, Phys. Rev. B 76 (2007) 014504.
[19] O. Dobrovolskiy, M. Huth, V. Shklovskij, Supercond. Sci. Technol. 23 (2010) 125014.
[20] A. Semenov, K. Il'in, M. Siegel, A. Smirnov, S. Pavlov, H. Richter, H.-W. Hübers, Supercond. Sci. Technol. 19 (2006) 1051.
[21] A. Engel, A. Semenov, H.-W. Hübers, K. Il'in, M. Siegel, Physica C 444 (2006) 12.
[22] K. Likharev, V. Semenov, IEEE Trans. Appl. Supercond. 1 (1991) 3.
[23] V. Moshchalkov, R. Wördenweber, W. Lang, Nanoscience and Engineering in Superconductivity, Springer-Verlag, Berlin-Heidelberg, 2010.
[24] J. Bardeen, M. Stephen, Phys. Rev. 140 (1965) A1197.
[25] M. Tinkham, Introduction to Superconductivity, 2004 Mineola, New York.
[26] J. Thornton, Annu. Rev. Mater. Sci. 7 (1977) 239.
[27] C. Flynn, J. Phys. F 18 (1988) L195.
[28] M. Huth, C. Flynn, Appl. Phys. Lett. 71 (1997) 2466.
[29] S. Prischepa, D. Montemurro, C. Cirillo, C. Attanasio, M. Salvato, V. Merlo, A. Lykov, A. Tsvetkov, Supercond. Sci. Technol. 19 (2006) 1124.